# $CO_2$-leakage-driven diffusiophoresis causes spontaneous accumulation of charged materials in channel flow

Suin Shim[a,1] and Howard A. Stone[a,1]

[a]Department of Mechanical and Aerospace Engineering, Princeton University, Princeton, NJ 08540

Edited by David A. Weitz, Harvard University, Cambridge, MA, and approved August 26, 2020 (received for review May 18, 2020)

**We identify a phenomenon where the onset of channel flow creates an unexpected, charge-dependent accumulation of colloidal particles, which occurs in a common-flow configuration with gas-permeable walls, but in the absence of any installed source of gas. An aqueous suspension of either positively charged (amine-modified polystyrene; a-PS) or negatively charged (polystyrene; PS) particles that flowed into a polydimethylsiloxane (PDMS) channel created charge-dependent accumulation 2 to 4 min after the onset of flow. We unravel the phenomenon with systematic experiments under various conditions and model calculations considering permeability of the channel walls and $CO_2$-driven diffusiophoresis. We demonstrate that such spontaneous transport of particles is driven by the gas leakage through permeable walls, which is induced by the pressure difference between the channel and the ambient. Since the liquid pressure is higher, an outward flux of gas forms in the flow. We also observe the phenomenon in a bacterial suspension of *Vibrio cholerae*, where the fluorescent protein (mKO; monomeric Kusabira Orange) and bacterial cells show charge-dependent separation in a channel flow. Such experimental observations show that diffusiophoresis of charged particles in an aqueous suspension can be achieved by having gas leakage through permeable walls, without any preimposed ion-concentration gradient in the liquid phase. Our findings will help resolve unexpected challenges and biases in on-chip experiments involving particles and gas-permeable walls and help understand similar configurations that naturally exist in physiological systems, such as pulmonary capillaries. We also demonstrate potential applications, such as concentrating and collecting proteins below the isoelectric point.**

microfluidics | diffusiophoresis | $CO_2$ leakage | protein purification

When a particle suspension flows at a constant flow rate in a microfluidic channel, we expect a steady flow of uniformly dispersed particles (1). Such particle-laden flow is ubiquitous in physiological and diagnostic systems (2–9). Here, we identify a phenomenon where the onset of channel flow creates an unexpected, charge-dependent accumulation of colloidal particles. With experiments and a model considering permeability of the channel walls (10–14) and $CO_2$-driven diffusiophoresis (15–17), we demonstrate that the spontaneous transport of particles is driven by gas leakage through permeable walls. Diffusiophoresis is a motion of particles under a concentration gradient of solute. Some previous studies demonstrate particle motion driven by dissolution of $CO_2$ in an aqueous phase (and generation of $H^+$, $HCO_3^-$, and $CO_3^{2-}$ ions) (15–17). In this article, we demonstrate and validate the migration of charged particles in the absence of any installed $CO_2$ source. Due to the pressure-driven flow, there is a flux of $CO_2$ from the liquid to the ambient, which creates an ion-concentration gradient in the flow. The unusual particle accumulation is also observed in a bacterial suspension of *Vibrio cholerae* cells, where a fluorescent protein and bacterial cells show charge-dependent separation in a channel flow.

We present our observations in multiple geometries, including straight and serpentine channels, a branching–merging network, and channels with grooves on the side walls. Moreover, we show that diffusiophoresis of charged particles (18, 19) can be achieved without any preimposed ion-concentration gradients in a channel flow and demonstrate potential applications to concentrating and collecting proteins below the isoelectric point. This limit of a small ion-concentration gradient is ubiquitous and is opposite from the high-salinity regime studied in ref. 20.

When a dilute suspension of positively charged (zeta potential $\zeta \approx 60$ mV) (21), micrometer-diameter particles flows into a serpentine microfluidic channel (width, height, and length are, respectively, $w = 250$ $\mu$m, $h = 70$ $\mu$m, and $\ell = 16$ cm) made of three sides polydimethylsiloxane (PDMS) and one side glass (Fig. 1*A*), we observed a nonuniform, transient particle focusing on top of the mean flow (Movie S1). We refer to this phenomenon as a "pulse" throughout the paper. The pulse is generated spontaneously several minutes after starting the flow. As the pulse is generated, it travels along the channel at a nearly constant speed that is much smaller than the mean flow velocity $\langle u \rangle$ (Fig. 1 *B* and *C*). Negatively charged particles do not

## Significance

Particle-laden flow is ubiquitous in physiological and diagnostic systems, where usually the particles (e.g., colloidal particles, cells, macromolecules, etc.) gain a nonzero net surface charge when suspended in an aqueous phase. Polydimethylsiloxane (PDMS) has been the most popular material used for microfluidic fabrications for the past two decades. Its high gas permeability is well appreciated, but the possible influence of gas leakage on the motion of charged particles has not been recognized. By systematic experiments and model calculations, we demonstrate that initial (early time) gas leakage through PDMS can create a charge-dependent accumulation of particles in common channel flows by diffusiophoresis and show that the phenomenon can be applied to concentrating and collecting proteins.

Author contributions: S.S. discovered the phenomenon and conceived the idea of $CO_2$-leakage-driven diffusiophoresis; S.S. and H.A.S. developed the hypothesis and the structure of the model; S.S. designed and performed all experiments, and conducted numerical calculations; S.S. and H.A.S. analyzed the experimental and numerical data; and S.S. and H.A.S. wrote the paper.

Competing interest statement: The authors declare no financial conflicts. H.A.S. is 50% owner of Phoresis, Inc., which is a startup seeking to utilize diffusiophoresis as a technology for removing particles from water. There are no competing interests with the ideas discussed in this paper.

This article is a PNAS Direct Submission.



[1]To whom correspondence may be addressed. Email: sshim@princeton.edu or hastone@princeton.edu.

This article contains supporting information online at https://www.pnas.org/lookup/suppl/doi:10.1073/pnas.2010011117/-/DCSupplemental.

First published October 2, 2020.

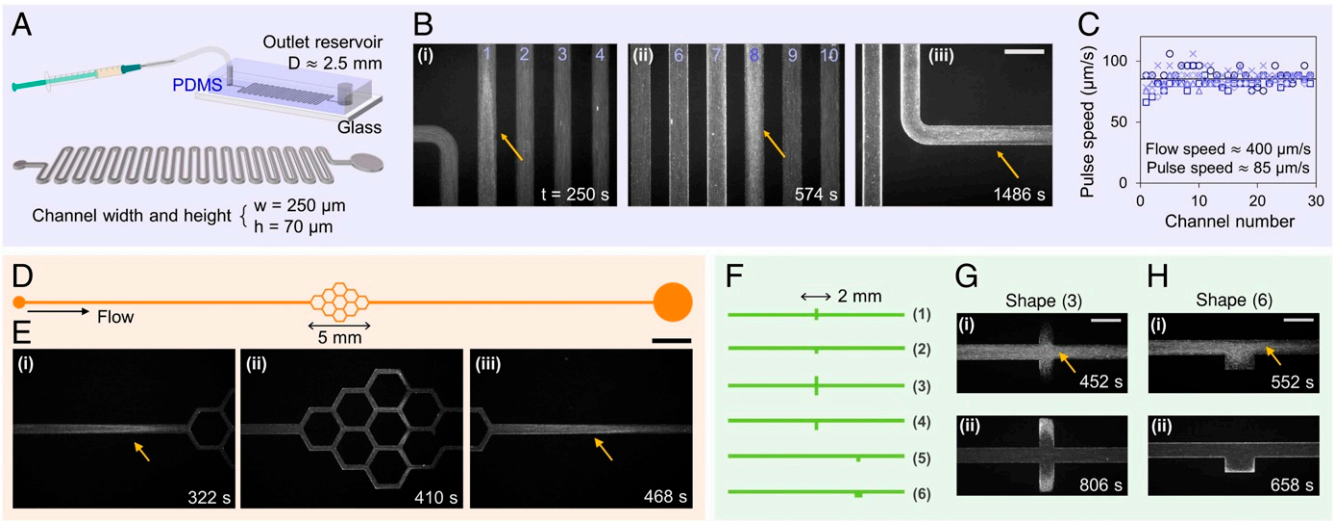


**Fig. 1.** Spontaneous pulse generation in various channel geometries. (*A*) Schematic of the first experimental setup (details in *Materials and Methods*) and channel geometry. Centerline length of the channel is $\ell = 16$ cm. (*B*) A pulse of particles in a single, serpentine channel, visualized with fluorescent images at different positions and times. The numbers are assigned to each section of the channel to measure the pulse speed. (*C*) Measurements of the pulse speed for five different experiments performed at a mean flow speed $\langle u \rangle \approx 400$ $\mu$m/s. The pulse speed is nearly constant along the channel, and its value is significantly smaller than the mean flow velocity. (*D*) Schematic of the geometry used for pulse experiments with a complex network. a-PS particles of diameter $d = 1$ $\mu$m are flowed into the channel and generated a pulse. (*E*) Time sequence of pulse images taken at different times and positions. (*E*, *ii*) When the pulse flows into the multiple-branch network, its position can be tracked by the change in the intensity along the branches. (*E*, *iii*) After the pulse flows through the network, it merges into one pulse again, and then flows downstream. (*F*) Schematics of the geometries used for pulse experiments with grooves. The first four channels have either asymmetric or symmetric grooves located halfway ($x = 2.5$ cm) along the channel, and the last two channels have asymmetric grooves located at $x \approx 3.5$ cm. (*G* and *H*) Time sequence images obtained from the geometries 3 and 6. For all channels with the grooves of different sizes and configurations, entrainment of accumulated particles into the grooves is observed after the pulse flowed past the grooves. [Scale bars: 500 $\mu$m (*B*), 1 mm (*D*), and 500 $\mu$m (*G* and *H*)]. All arrows indicate the location of the pulse.

create a pulse, but accumulate near the permeable side walls (discussed later; see Fig. 4).

Also, we observed pulse generation in channels with a complex network (Fig. 1 *D* and *E* and Movie S2) and grooves (Fig. 1 *F*–*H* and Movie S3). In the branching–merging network, the focused particles on a pulse separated into the subchannels (Fig. 1 *E*, *ii*), then merged at the outlet of the network (Fig. 1 *E*, *iii*). In the channels with grooves (Fig. 1*F*), we observed a pulse, followed by entrainment of particles in the grooves as the pulse traveled downstream (Fig. 1 *G* and *H*).

To the best of our knowledge, the generation of this type of nonuniformity, or pulse, has not been documented previously, but its ubiquity and ready generation mean that it may influence many colloidal measurements that occur in physiological and diagnostic systems. Therefore, we establish a hypothesis for the origin of the pulse and provide systematic proof with experiments and a model calculation (*SI Appendix*). In particular, we hypothesize that the pulse is induced by $CO_2$-driven diffusiophoresis of particles. Under a gradient of $CO_2$ concentration (or the ions $H^+$ and $HCO_3^-$) in an aqueous suspension of charged particles, the particles move either up or down the gradient, depending on their charge (15–17). In our system, which is similar to most designs currently utilized in laboratories, as well as common portable devices, the $CO_2$ concentration gradient can be created by leakage of gas through PDMS, which is induced by a pressure gradient across the wall material.

Two observations about pulse generation are: 1) There is initial focusing of particles within several millimeters downstream of the inlet, and 2) the accumulated particles (pulse) travel downstream at a constant speed that is significantly smaller than the mean flow speed (Fig. 1*C*). Once the flow starts, there is an increase in the liquid pressure, which we hypothesize establishes a pressure gradient across the PDMS wall (Fig. 2 *A* and *B*). As a result, a nonzero flux of liquid and gas (that is already dissolved in the liquid phase) may form across the channel wall. However, since PDMS has very small permeability to liquid, only gas has an effective flux. In the liquid, as the predissolved gas (15) is lost to the surroundings, a concentration gradient of gas forms. A gradient in dissolved $CO_2$ in water can create the motion of charged particles, i.e., diffusiophoresis. In our experiments, the positively charged amine-modified polystyrene particles (a-PS), as a result of $CO_2$-driven diffusiophoresis, move toward higher $CO_2$ concentration (Fig. 2 *A* and *B*). Further downstream, the particles accumulate near the glass surface, which is observed as the initial focusing (Fig. 2 *B* and *C*). The focused particles then flow along the channel at a constant speed (Fig. 2*C*), much slower than the mean, since the particles are close to the glass wall.

To verify the gas-leakage hypothesis, we performed control experiments with different channel materials: ultraviolet (UV)-curable epoxy and glass. In the impermeable epoxy channel (22), which has the same dimensions as the original experiments, we set up the same flow ($\langle u \rangle = 400$ $\mu$m/s) and then chose one position to take the fluorescent images. Another steady-flow experiment was done in a straight glass capillary with a square cross-section (200 $\mu$m $\times$ 200 $\mu$m). In both epoxy and glass channels, we did not observe any pulse or focused particles passing the fixed position during $\sim$30 min of recording time (Fig. 2 *D* and *E* and Movie S4). Therefore, we conclude that the spontaneous pulse generation is related to the gas permeability of the PDMS walls in the system.

In the PDMS channel, gas is lost through three permeable walls (Fig. 2*F*), and, thus, a-PS particles are expected to migrate away from the PDMS walls and toward the glass surface by diffusiophoresis. Confocal microscopy (Leica TCS SP5) experiments (Fig. 2 *G*–*I* and Movie S5) showed the cross-sectional view of pulse experiments, both in normal and upside-down configurations, and visualized that the particles focus near the glass slide. The result that the pulse flows near the glass slide suggests that the particle motion dominates any buoyancy effects and is

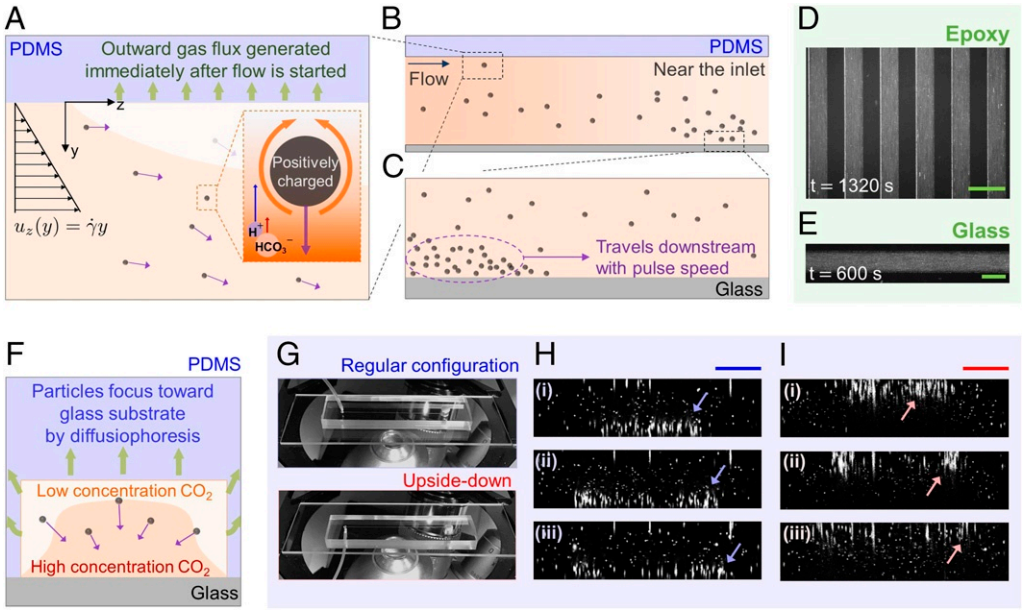


**Fig. 2.** The hypothesis of $CO_2$-driven diffusiophoresis. (*A–C*) Schematic of the inlet region of a channel, which describes $CO_2$ loss through PDMS and induced diffusiophoresis of particles. For the model (*SI Appendix*), we assume a constant gas flux and shear flow approximation. (*A*, *Inset*) Diffusiophoresis of a particle is described with different diffusivities of $H^+$ and $HCO_3^-$. (*B*) Schematic of a channel flow. (*C*) Schematic showing the accumulated particles near the glass substrate. (*D* and *E*) Control experiments in gas-impermeable channels: epoxy channel (*D*) and a glass capillary (*E*). No pulse was observed (Movie S4). (*F*) Schematic of a cross-sectional view of the channel flow, describing diffusiophoretic focusing of a-PS particles. (*G–I*) Experiments with PDMS channels in regular and upside-down configurations. In both configurations, we observe that particles are focused near the glass substrate. The time increments between two successive images are, respectively, 8 s (*H*) and 16 s (*I*). [Scale bars: 500 $\mu$m (*D*), 200 $\mu$m (*E*), and 50 $\mu$m (*H* and *I*).] All arrows indicate the position of the pulse.

consistent with the directionality predicted from the diffusiophoresis hypothesis.

In a channel, the pulse speed does not change as it travels downstream, even though, for a longer channel, the absolute liquid pressure is higher near the inlet. In a rectangular channel, the pressure gradient $\frac{\Delta p_L}{\ell} \propto \frac{\mu\langle u\rangle}{h^2}$, and so the liquid pressure $p_L$ relative to the atmosphere ($p_a$) is $p_L - p_a = \alpha\frac{\mu\langle u\rangle}{h^2}(\ell - x)$, where $\mu$, $\alpha$, and $x$ are, respectively, the viscosity of liquid, a constant, and the coordinate along the flow. Our observations of the pulse speed proportional to the mean flow speed (Fig. 3*A*) indicate that the pulse speed is related to the pressure *gradient* in the channel rather than the absolute liquid pressure. Moreover, the negligible dependence on the length of the channel $\ell$ (Fig. 3*B*) suggests that the main event of pulse generation occurs only near the inlet, at the early stage of the flow (Fig. 2 *A* and *B*). Initial focusing of the particles near the inlet, followed by a constant-speed movement of the pulse, indicates that the particle distribution at the inlet reaches steady state after the focusing (*SI Appendix*, section III).

According to the diffusiophoresis hypothesis, negatively charged polystyrene (PS) particles are expected to accumulate toward the sides with PDMS walls (*SI Appendix*, section II). The side-wall accumulation of negatively charged particles can be visualized in a channel with a groove (Fig. 4 *A–D* and Movie S6) by using an inverted microscope (Leica DMI4000B). We performed experiments in PDMS and UV epoxy channels with the same geometry (Fig. 4 *A* and *B*). In the groove, we observed penetration of particle streamlines and entrainment of PS particles both in PDMS and epoxy channels (23, 24). However, in the PDMS channel, there were more particles entering the groove, which were from side-wall accumulation (Fig. 4 *A* and *D*). The intensity plot across the main channel (Fig. 4*C*) shows that there are more particles on the PDMS side walls ($x = 0$ and $x = 0.25$ mm) than the epoxy walls. An increase in the particle concentration in the groove (Fig. 4*D*) clearly shows that there are extra particles from the side wall of the PDMS channel, supporting our hypothesis.

We argue that our results are consistent with a mechanism where particle diffusiophoresis is created by a flow-generated $CO_2$-concentration gradient and so potentially impact similar microscale measurement devices with gas-permeable walls. To describe diffusiophoresis, we typically need the diffusiophoretic mobility of a particle $\Gamma_p$, concentration of ions $c_i$, and the diffusivity of $CO_2$ in water $D_c$. An estimate for the diffusiophoretic speed and so the distance $\ell_\perp$ characteristic of the transverse motion of particles in a channel of length $\ell$ is then $\ell_\perp \approx \frac{\ell}{\langle u\rangle}\Gamma_p \nabla \ln c_i \approx \frac{\Gamma_p}{\sqrt{D_c/\dot{\gamma}}}\frac{\ell}{\langle u\rangle} \approx O(10^{-3} - 10^{-2})$ m, much larger than height, which confirms that it is possible for

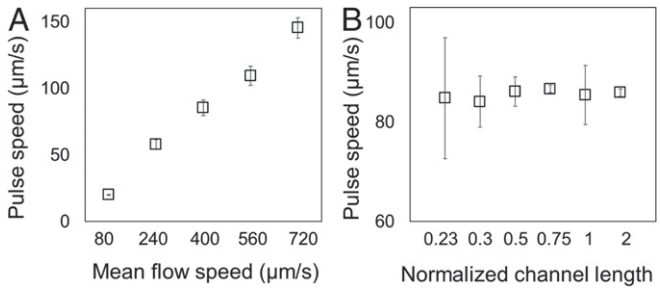


**Fig. 3.** Pulse-speed measurements done at different mean flow speeds (*A*) and in the channels with different lengths (*B*). (*A*) The speed of a pulse is linearly proportional to the flow speed. (*B*) The average pulse speed is almost independent of the channel length, when the flow speed is constant ($\langle u\rangle = 400$ $\mu$m/s). The normalized channel length 1 corresponds to the serpentine channel in Fig. 1*A*; $\ell = 16$ cm. The normalized lengths 0.23 and 0.3 are that of straight channels.

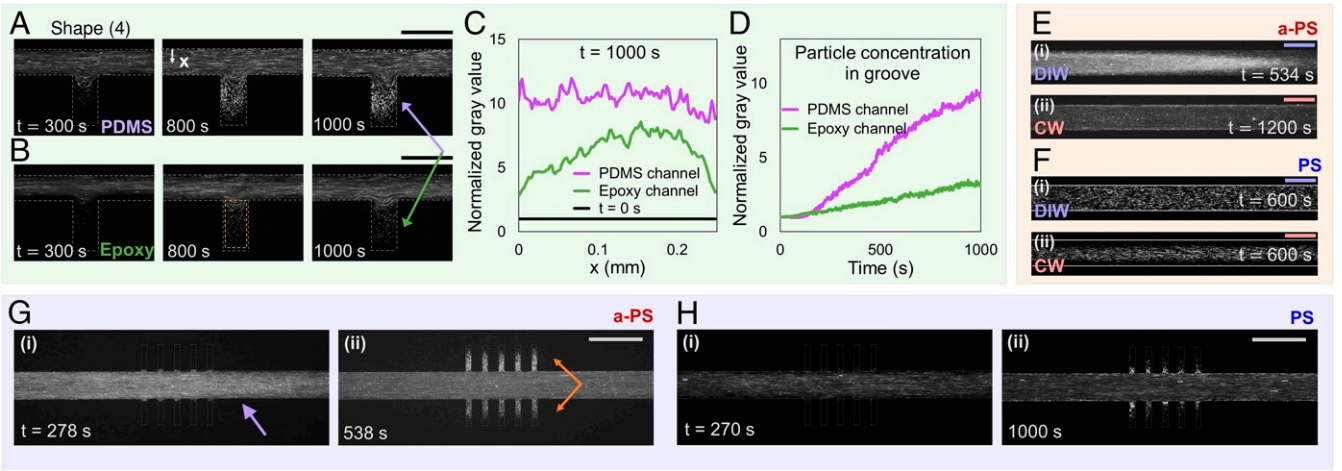


**Fig. 4.** Behavior of PS and a-PS particles under various conditions. (*A–D*) PS particles flowing past a groove (shape 4 from Fig. 1) in PDMS (*A*) and epoxy (*B*) channels. In both systems, penetration of particle paths into the groove is observed. Without gas-permeable walls, there is no additional entrainment of wall-accumulated particles. (*A* and *B*) The arrows indicate entrainment of PS particles in the grooves. (*C* and *D*) Intensity measurement along the channel (*C*) and in the groove (*D*). (*E* and *F*) Effect of $CO_2$ flux on the particle diffusiophoresis. (*E*) a-PS particles flowing in DIW (*i*) and CW (*ii*) PDMS channels, showing that the particle focusing is affected by reverse $CO_2$ flux. (*F*) PS particles flowing in DIW (*i*) and CW (*ii*) PDMS channels. In the CW PDMS channel, the PS particle stream is detached from the side walls. (*G* and *H*) a-PS (*G*) and PS (*H*) particles flowing past multiple grooves. (*G*) A pulse is generated (*i*), and the accumulated particles are entrained into the grooves (*ii*). (*G*) The purple arrow (*i*) indicates the pulse, and the orange arrows (*ii*) indicate entrainment of a-PS particles in the grooves. (*H*) PS particles that accumulate along the side walls are also entrained in the grooves. [Scale bars: 300 $\mu$m (*A* and *B*), 200 $\mu$m (*E* and *F*), and 500 $\mu$m (*G* and *H*).]

particles to focus toward the glass substrate while flowing through a channel of length $\ell$ (*SI Appendix*, section III).

In order to prove that the gas which causes leakage-driven diffusiophoresis is $CO_2$, we performed experiments using deionized-water-saturated (DIW) and carbonated-water-saturated (CW) PDMS channels (Fig. 4 *E* and *F* and Movie S7). In the DIW channels, a-PS particles created a pulse and PS particles showed side-wall accumulation, whereas in the CW channels, there was no pulse for a-PS particles, and the PS particle stream detached from the side walls. This set of experiments demonstrates that the unusual accumulation of charged particles is suppressed by having $CO_2$-concentrated surroundings, supporting our hypothesis that the phenomenon is driven by $CO_2$ leakage. These experiments also show that the vapor transport through PDMS is not a major parameter for pulse generation.

The effect of varying gas flux through PDMS was studied experimentally by controlling the thickness $H$ and gas permeability $P$ of PDMS, as the gas flux through a membrane $j \propto P/H$ (*SI Appendix*, section III). The permeability of PDMS was varied by changing the mixing ratio between the monomer and the cross-linker at the soft-lithography stage (10). For both control experiments (Fig. 5), we obtained that the pulse speed was faster for larger gas-flux conditions, even though the liquid flow condition was maintained consistent over the experiments (channel dimension of Fig. 1*A*, with the flow speed $\langle u \rangle = 400$ $\mu$m/s). When the 4-mm-thick PDMS channels made with a 10:1 mixing ratio were degassed under vacuum (*Materials and Methods*) before the experiments, the measured pulse speed was $\approx 103$ $\mu$m/s. Degassed PDMS is prone to higher absorption of $CO_2$ from both the ambient and the liquid flow. Even under this condition, the liquid pressure is higher than the ambient, and we observed a pulse that was faster due to the increased outward gas flux. Our model calculations in *SI Appendix*, section III-F show that the smaller gas flux through PDMS resulted in a particle accumulation that was closer to the glass slide, which caused a smaller travel speed of pulse.

We further visualized different groove-entrainment behaviors of a-PS and PS particles in a channel with multiple grooves (Fig. 4 *G* and *H* and Movie S8). We observed that the particles in the pulse (a-PS) entrained deeper into the grooves compared to the PS particles from the side wall. This observation suggests possible charge-dependent particle collection in side-wall reservoirs. The complete step-by-step validation is reported in *SI Appendix*, sections II and III.

Next, we studied a bacterial suspension of wild-type *V. cholerae* in the channel flow, as the solution was recognized as a natural mixture of negatively charged (cells) and positively charged (fluorescent protein mKO; monomeric Kusabira Orange in the surrounding liquid) materials (17, 25–27). In ref. 17, it is suggested that the background fluorescent protein undergoes $CO_2$-driven diffusiophoresis. When a suspension of *V. cholerae* wild-type cells in 10 % M9 solution (*Materials and Methods*) was flowed into the PDMS channel with multiple grooves (Fig. 6 *A–C* and Movie S10), a pulse was generated, and then part of the pulse entrained into the grooves. However, the bacterial cells are

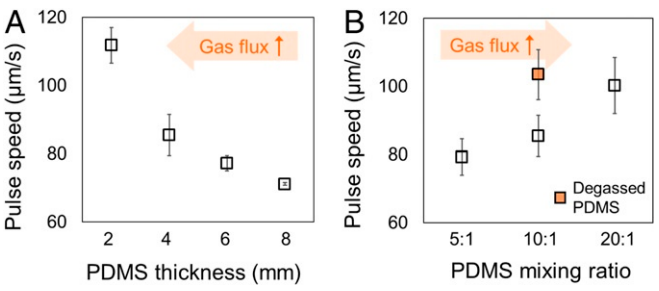


**Fig. 5.** Pulse-speed measurements under different gas-flux conditions. While the liquid-flow condition inside the channel is maintained as identical (channel dimension of Fig. 1*A*, with $\langle u \rangle = 400$ $\mu$m/s), the gas flux through PDMS walls is varied by changing the thickness $H$ of PDMS (gas flux $\propto 1/H$) (*A*) and varying the mixing ratio between monomer and the cross-linker at the soft lithography stage (this tunes the gas-permeability $P$) (*B*). (*A*) The mixing ratio is 10:1. (*B*) The PDMS thickness is 4 mm. In both sets of experiments, the pulse speed is higher with the larger gas flux. The orange arrows indicate how the gas flux changes as the independent variable in the figure changes.

negatively charged, so we do not expect pulse generation. In the grooves (Fig. 6*B*), we observed that the material that created the pulse was the background fluorescent protein mKO. Pulse generation was suppressed in the CW channel with grooves (Fig. 6*D*). mKO accumulated due to $CO_2$-leakage-driven diffusiophoresis in channel flow similar to a-PS particles; more control experiments showing this analogy are reported in *SI Appendix*, section II-B.

Pulse generation of protein molecules can be further applied to a microfluidic protein extraction (28–30). In the protein-purification systems, it is often challenging, or it requires extra steps, to concentrate target proteins to a desired amount. If the target protein in a liquid phase can generate a pulse by flowing in gas-permeable channels, the protein can be concentrated without any pre-imposed external driving force on the initially dilute solutions. If a straight channel was used, a pulse can be simply collected at the outlet of the channel. Otherwise, we can also design side-wall reservoirs to collect the pulse materials (Fig. 6 *E* and *F*). Since the size of mKO is $O$ (1 to 10) nm, the molecules can disperse ($D_p \approx 10^{-10}$ m$^2$/s; Stokes–Einstein diffusivity) in the microfluidic channel and be collected at one end. However, the concentration of collected protein does not increase by simple dispersion (Fig. 6 *E*, *i–iii*).

We believe that the effect of deformable elastic walls is negligible, as the pulse generation is highly dependent on the particle charge, flow condition, and wall permeability. Also, the wall charge ($\zeta \approx -100$ mV) (31) has negligible effect on the pulse generation (a-PS) or side-wall accumulation (PS), since the phenomenon is in the opposite direction to the particle attraction to (or repulsion from) the walls (*SI Appendix*, section V).

Our systematic experiments have shown that there is an unexpected, spontaneous accumulation of charged particles in channel flows due to $CO_2$ leakage. We are aware that microfluidic experiments involving diffusiophoresis of particles are not linear with the changes in scales, and, thus, the observations of spontaneous particle accumulation may not be geometrically identical in different systems. We are currently working to understand the details of the flow structure and the particle distribution in the system. We believe that our findings will impact the science of relevant systems with gas exchange, such as particulate-matter studies or drug deliveries in pulmonary capillaries. Also, our observations on the diffusiophoresis without a pre-imposed ion-concentration gradient may contribute to improved particle transport in confined geometries. Finally, the approach can provide systematic tools for experimental studies involving charged materials, such as separation, phoresis, and dispersion. The application for a protein-purification system is one example.

## Materials and Methods

**Main Experiments.** The experimental setup (Fig. 1*A*) includes three parts—channel preparation, particle suspension preparation, and setting up the flow.

***PDMS microfluidic channel.*** For the microfluidic channel used in the experiments, we followed the standard soft lithography. As we wanted to control all of the properties, we fixed the recipe as below.

1.) Mix the monomer and curing agent with 10:1 weight ratio, then keep the mixture under vacuum for 30 min.
2.) Take out the mixture from the vacuum chamber, pour it onto the petri dish containing a mold, and then keep everything under vacuum for another 30 min.
3.) Put the mold with PDMS in the 75 °C oven and bake it for 3 h.
4.) Maintain at room temperature for 30 min to cool down the PDMS channel and mold.
5.) Cut the channel, plasma-treat the channel surface and glass slide for 10 s each with the laboratory corona treater, and then bond to each other.
6.) Put the bonded channels on a 120 °C hot plate for 30 min.
7.) Maintain the channels for 1 h at room temperature and then use.

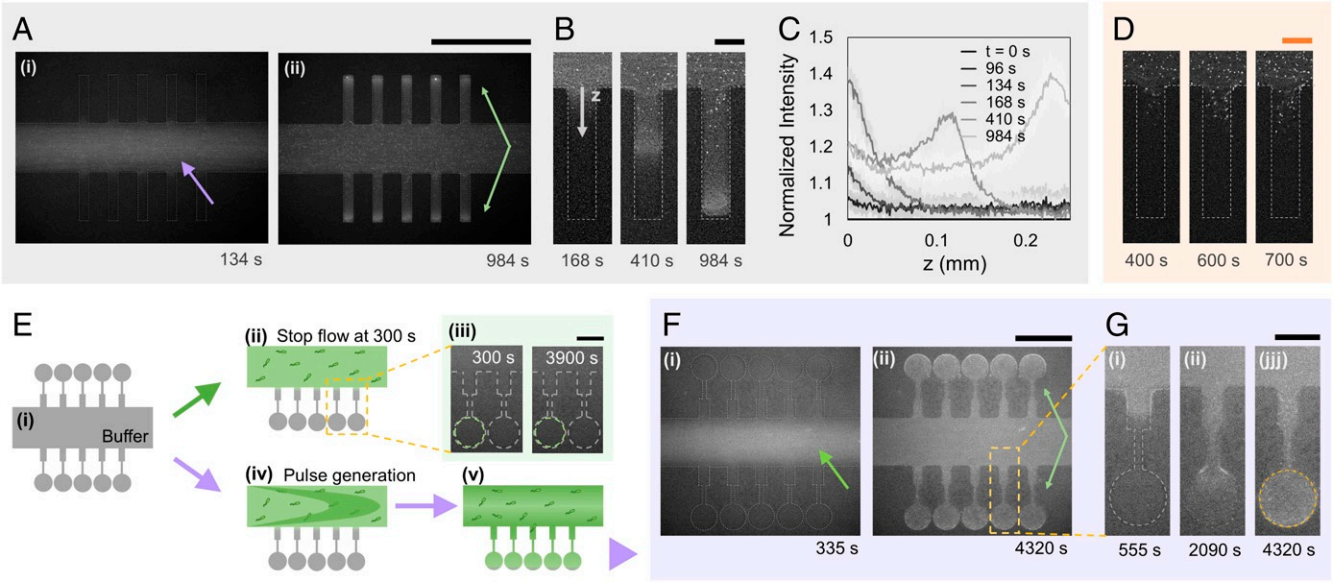


**Fig. 6.** Bacterial suspension (*V. cholerae*) flowing past multiple grooves in dry (*A–C*) and CW (*D* and *E*) PDMS channels. (*A*) We observe one bright signal (pulse) that travels downstream and entrains its portion into the grooves. (*B*) We observe that the deep-entrained bright signal in the grooves is different from the cell entrainment. (*C*) Intensity measurements along the grooves (10-groove average). (*D*) In the CW-saturated PDMS channel, only slight entrainment of the cells is observed. (*E*) Schematics showing two different protein collection scenarios. (*E*, *ii*) Since the fluorescent protein mKO is *O* (1 to 10) nm in size, it is expected to be dispersed into the grooves faster than the bacterial cells by pure diffusion. (*E*, *iii*) Experimental images showing the small reservoirs at the end of the grooves. No significant collection of mKO is achieved. (*E*, *iv* and *v*) In the presence of flow and pulse generation, entrainment of focused mKO, and, thus, collection of highly concentrated mKO, is possible in the grooves. (*F*) Experimental images showing the generation of mKO pulse, followed by deep entrainment of concentrated mKO into the grooves. (*G*) Magnified images of one groove showing effective mKO extraction from the bacterial suspension. (*A* and *F*) The arrows indicate the position of the pulse and the entrainment of the charged materials into the grooves from the pulse. [Scale bars: 500 $\mu$m (*A*), 50 $\mu$m (*B* and *D*), 100 $\mu$m (*E*, *iii*), 300 $\mu$m (*F*), and 100 $\mu$m (*G*).]

As a result of the above steps, we obtained 4-mm-thickness PDMS microfluidic channels with our single-stream, serpentine design. To avoid the uncontrollable effect of an outlet tube on the main flow, we chose to collect the liquid in an outlet reservoir (Fig. 1*A*).

***Particle-suspension preparation.*** For positively charged particles, we used a suspension of a-PS particles (Sigma-Aldrich, 1-$\mu$m diameter, batches MKBX6372V and MKCF6014), and the concentration was kept at 0.036 vol% for all experiments. For negatively charged particles, we used PS particles (Thermo Fisher Scientific, 1 $\mu$m diameter), and the concentration was 0.03 vol%.

***Experiment setup.*** After the channel and the particle suspension were prepared, we first filled the entire channel with deionized (DI) water at a flow rate of 200 $\mu$L/h, and then the channel remained under atmospheric conditions for 2 min. The 1-mL syringe filled with a 0.5-mL particle suspension was connected with polytetrafluoroethylene (PTFE) tubing to the channel. PTFE tubing was chosen because it has relatively low permeability to $CO_2$ compared to low-density polyethylene tubes (32), which are commonly used in microfluidic experiments. The particle suspension was flowed into the channel at 25 $\mu$L/h, corresponding to the mean flow speed $\langle u \rangle = 400$ $\mu$m/s (this is the flow rate we chose for the main experiments). The pulse (a-PS) and side-wall accumulation (PS) can also be generated by directly flowing a particle suspension into the initially empty channel (*SI Appendix*, section IV), but for the consistent experimental conditions, we chose to fill the channel with DI water before introducing the particle suspension.

**Control Experiments.**

***UV epoxy channel.*** The epoxy channel used in the experiments is made with a UV-curable epoxy (catalog no. NOA81, Norland Products) using the microfluidic sticker technique (33). Similar to the main experiments, we filled the channel with DI water at a flow rate of 200 $\mu$L/h. After 2 min, the syringe filled with a particle suspension was connected with PTFE tubing to the channel. The experiment was run at 25 $\mu$L/h.

***Glass capillary.*** A 8-cm-long glass capillary with 200 $\mu$m $\times$ 200 $\mu$m cross-section (VitroCom) was attached to a glass slide and connected to the PTFE tubing. A particle suspension was flowed into the capillary at 57 $\mu$L/h, which corresponds to the mean flow speed $\langle u \rangle = 400$ $\mu$m/s.

***Confocal microscopy.*** For the confocal microscopy (Leica TCS SP5), a straight channel with the length $\ell = 3.6$ cm was used. For imaging the cross-sectional view, we chose a position at 3 cm downstream from the inlet (for both regular and the upside-down configurations).

***CW PDMS.*** We made the PDMS channels with the method described in *PDMS Microfluidic Channel*. Then, we stored the channel in a 50-mL tube filled with carbonated water for 24 h. The carbonated water is made by a commercial carbonator (SodaStream) with DI water. Liquid in the tube was replaced once with fresh carbonated water after 12 h. After 24 h, the PDMS channel was saturated with carbonated water. We flowed non-bubbly carbonated water into the channel at a flow rate of 200 $\mu$L/h for 1 min, and then ran the experiment by introducing a particle suspension at 25 $\mu$L/h.

***Degassed PDMS channel.*** We made the PDMS channels with the method described in *PDMS Microfluidic Channel*. Then, the channels were stored under vacuum for 18 h and brought back to the atmospheric pressure before each experiment. The particle flow (25 $\mu$L/h) was switched on within 1 min after the vacuum was removed.

**Bacterial Suspension.** *V. cholerae* strains (17) were grown overnight at 37 °C in liquid Luria–Bertani (LB) with shaking. After 20 h of growth in LB, the sample was centrifuged at $\approx 500 \times g$ for 7 to 8 min. After removing supernatant, strains were resuspended in 5 mL of M9 minimal salt solution for an additional 2 h (at 37 °C, with shaking) to achieve exponential phase ($OD_{600} \approx 1$). Then, for the $CO_2$-driven diffusiophoresis experiments, the suspension was centrifuged at $\approx 500 \times g$ for 7 to 8 min and resuspended into 5 mL of 10 % M9 minimal salt solution to achieve optical density at 600 nm = 0.23.

**Data Availability.** Data related to this work are available on DataSpace (DOI: 10.34770/7607-9f26).

**ACKNOWLEDGMENTS.** We thank Janine K. Nunes for her help with the confocal microscopy; Orest Shardt for in-depth discussion on $CO_2$-driven diffusiophoresis; Jesse T. Ault and Bhargav Rallabandi for discussions on the solitons; Andrej Kosmrlj for useful discussion on the chemical potential; and the Bassler Lab and Jing Yan for providing the *V. cholerae* strains. This work was supported by NSF Grant CBET-1702693.

1. H. A. Stone, A. D. Stroock, A. Ajdari, Engineering flows in small devices: Microfluidics toward a lab-on-a-chip. *Annu. Rev. Fluid Mech.* **36**, 381–411 (2004).
2. J. A. Potkay, The promise of microfluidic artificial lungs. *Lab Chip* **14**, 4122–4138 (2014).
3. R. Fishler, P. Hofemeier, Y. Etzion, Y. Dubowski, J. Sznitman, Particle dynamics and deposition in true-scale pulmonary acinar models. *Sci. Rep.* **5** 14071 (2015).
4. J. Tenenbaum-Katan, A. Artzy-Schnirman, R. Fishler, N. Korin, J. Sznitman, Biomimetics of the pulmonary environment in vitro: A microfluidics perspective. *Biomicrofluidics* **12**, 042209 (2018).
5. P. M. Valencia, O. C. Farokhzad, R. Karnik, R. Langer, Microfluidic technologies for accelerating the clinical translation of nanoparticles. *Nat. Nanotechnol.* **7**, 623–629 (2012).
6. J. Ahn *et al.*, Microfluidics in nanoparticle drug delivery; from synthesis to preclinical screening. *Adv. Drug Deliv. Rev.* **128**, 29–53 (2018).
7. D. Li *et al.*, Fluorescent reconstitution on deposition of $PM_{2.5}$ in lung and extrapulmonary organs. *Proc. Natl. Acad. Sci. U.S.A.* **116**, 2488–2493 (2019).
8. F. Schulze *et al.*, Air quality effects on human health and approaches for its assessment through microfluidic chips. *Genes* **8**, 244–269 (2017).
9. F. Kiessling, M. E. Mertens, J. Grimm, T. Lammers, Nanoparticles for imaging: Top or flop? *Radiology* **273**, 10–28 (2014).
10. A. Lamberti, S. L. Marasso, M. Cocuzza, PDMS membranes with tunable gas permeability for microfluidic applications. *RSC Adv.* **4**, 61415–61419 (2014).
11. K. Berean *et al.*, The effect of crosslinking temperature on the permeability of PDMS membranes: Evidence of extraordinary $CO_2$ and $CH_4$ gas permeation. *Separ. Purif. Technol.* **122**, 96–104 (2014).
12. G. Firpo, E. Angeli, L. Repetto, U. Valbusa, Permeability thickness dependence of polydimethylsiloxane (PDMS) membranes. *J. Membr. Sci.* **481**, 1–8 (2015).
13. D. A. Markov, E. M. Lillie, S. P. Garbett, L. J. McCawley, Variation in diffusion of gases through PDMS due to plasma surface treatment and storage conditions. *Biomed. Microdevices* **16**, 91–96 (2014).
14. T. C. Merkel, V. I. Bondar, K. Nagai, B. D. Freeman, I. Pinnau, Gas sorption, diffusion, and permeation in poly(dimethylsiloxane). *J. Polym. Sci. B* **38**, 415–434 (2000).
15. S. Shim, "Interfacial flows with heat and mass transfer," PhD thesis, Princeton University, Princeton, NJ (2017).
16. S. Shin, O. Shardt, P. B. Warren, H. A. Stone, Membraneless water filtration using $CO_2$. *Nat. Commun.* **8**, 15181 (2017).
17. S. Shim *et al.*, $CO_2$-driven diffusiophoresis for removal of bacteria. arXiv:2009.07081 (16 September 2020).
18. D. C. Prieve, J. L. Anderson, J. P. Ebel, M. E. Lowell, Motion of a particle generated by chemical gradients. Part 2. Electrolytes. *J. Fluid Mech.* **148**, 247–269 (1984).
19. B. Abecassis, C. Cottin-Bizonne, C. Ybert, A. Ajdari, L. Bocquet, Boosting migration of large particles by solute contrasts. *Nat. Mater.* **7**, 785–789 (2008).
20. D. C. Prieve, S. M. Malone, A. S. Khair, R. F. Stout, M. Y. Kanj, Diffusiophoresis of charged colloidal particles in the limit of very high salinity. *Proc. Natl. Acad. Sci. U.S.A.* **116**, 18257–18262 (2019).
21. P. Bihari *et al.*, Optimized dispersion of nanoparticles for biological in vitro and in vivo studies. *Part. Fibre Toxicol.* **5**, 14 (2008).
22. A. Gerlach, W. Keller, J. Schulz, K. Schumacher, Gas permeability of adhesives and their application for hermetic packaging of microcomponents. *Microsyst. Technol.* **7**, 17–22 (2001).
23. F. Pan, A. Acrivos, Steady flows in rectangular cavities. *J. Fluid Mech.* **28**, 643–655 (1967).
24. S. Battat, J. T. Ault, S. Shin, S. Khodaparast, H. A. Stone, Particle entrainment in dead-end pores by diffusiophoresis. *Soft Matter* **15**, 3879–3885 (2019).
25. S. Kabir, S. Ali, Characterization of surface properties of *Vibrio cholerae*. *Infect. Immun.* **39**, 1048–1058 (1983).
26. T. Vissers *et al.*, Bacteria as living patchy colloids: Phenotype heterogeneity in surface adhesion. *Sci. Adv.* **4**, eaao1170 (2018).
27. S. Karasawa, T. Araki, T. Nagai, H Mizuno, A. Miyawaki, Cyan-emitting and orange-emitting fluorescent proteins as a donor/acceptor pair for fluorescence resonance energy transfer. *Biochem. J.* **381**, 307–312 (2004).
28. J. C. Janson, *Protein Purification: Principles, High Resolution Methods, and Applications* (John Wiley & Sons, New York, NY, 2011).
29. A. Persat, L. A. Marshall, J. G. Santiago, Purification of nucleic acids from whole blood using isotachophoresis. *Anal. Chem.* **81**, 9507–9511 (2009).
30. A. Rogacs, L. A. Marshall, J. G. Santiago, Purification of nucleic acids using isotachophoresis. *J. Chromatogr. A* **1335**, 105–120 (2014).
31. B. J. Kirby, E. F. Hasselbrink, Jr., Zeta potential of microfluidic substrates: 2. Data for polymers. *Electrophoresis* **25**, 203–213 (2004).
32. Cole-Parmer, Tubing Selection Guide (2018). https://www.coleparmer.com/tech-article/tubing-selection-guide. Accessed 3 December 2018.
33. D. Bartolo, G. Degré, P. Nghe, V. Studer, Microfluidic sticker. *Lab Chip* **8**, 274–279 (2008).